Preprints, 10th IFAC International Symposium on
Advances in Automotive Control
Columbus, Ohio, USA, August 28-30, 2022

Functional Stochastic Modeling of Empirical Knock Sensor Signals

James.C. Peyton Jones*, Vatsal Patel

Center for Nonlinear Dynamics & Control, Villanova University, Villanova, PA 19085
**e-mail: james.peyton-jones@villanova.edu*

Abstract: Knock behaves a cyclically random process but also excites deterministic knock resonant behavior within any given cycle. While individual instances of the resonant response are readily acquired, the stochastic / cyclic variations of such signals (which also reflect the underlying knock process) are harder to quantify. In this work, a more complete model of this process is developed, capturing both the cyclic variability in the knock response as well as its functional resonant behavior. A recently developed alignment process is first used to evaluate the characteristic ensemble mean knock 'signature' of the data. A functional linearization about this ensemble mean is then used to decompose and model cyclic variations in terms of small variations in amplitude, frequency and phasing of the signal. The model is fitted to the data, encapsulating the stochastic variation of the knock signal within the stochastic variation of the estimated parameters. A residual analysis used to assess the goodness of fit as a function of crank angle, and the distribution and covariance of the estimated parameters is discussed.

Keywords: Spark Ignition; Cylinder Pressure; Stochastic Modeling; Knock.

1. INTRODUCTION

Abnormal 'knocking' combustion is well known to generate impulsive and damaging increases in temperature and pressure within the cylinder, together with associated acoustic resonances in the combustion chamber, (Draper, 1938; Heywood, 1988). Detection and quantification of these resonances is one of the most commonly used methods to obtain a scalar knock intensity feedback signal for knock control purposes, (Lee, Hwang, Lim, Jeon, & Cho, 1998; Millo & Ferraro, 1998; Naber, Blough, Frankowski, Goble, & Szpytman, 2006; Shahlari & Ghandhi, 2012). The resonant frequencies, and their dependence on gas temperature, are readily predicted from theory, (Draper, 1938; Scholl, Davis, Russ, & Barash, 1998), but the precise time history of knock onset, growth, and decay is harder to predict or simulate based purely on the underlying physics of the process, (Brecq & Le Corre, 2005; Di Gaeta, Giglio, Police, & Rispoli, 2013; Pan, Shu, & Wei, 2014). Furthermore, knock is widely recognized as approximating a cyclically independent random process, (Jill. M. Spelina, Peyton Jones, & Frey, 2014), and the resultant knock signals therefore vary significantly from cycle to cycle, even under nominally steady state conditions. For empirically based studies, this makes it hard to characterize or quantify observed knock waveforms in any rigorous / repeatable way. Typical studies illustrate single instances of knocking or non-knocking cycles to highlight specific knock-related features, but these instances may not be generalizable. A statistical approach may provide a more reliable quantification of the process, capturing both the resonant characteristics of the signal as well as the cyclic / random characteristics of the knock process itself.

Recent work has therefore aimed to model the stochastic distribution from which individual knock instances are drawn, (J. C. Peyton Jones & Shayestehmanesh, 2021). These distributions are stationary with respect to cycle number (under steady state conditions) but vary as a function of time / crank angle. However, random phasing of knock onset from one cycle to the next also means that the crank-angle dependent properties are not naturally aligned with one another. Simple averaging across cycles, for example, therefore causes the resonant characteristics that are visible in individual traces, to vanish (along with other random noise) in the resultant ensemble mean. In reference (J. Peyton Jones & Patel, 2021), the data were therefore phase-aligned using a cross-correlation technique relative to a strongly knocking reference cycle, and the statistical properties of the resonant knock process could then be seen more clearly. In particular, it was shown that the data possessed a clear ensemble mean resonant knock 'signature', and that the shape of the distribution at any given crank angle could be modeled parametrically as a mixture of two Gaussian processes representing the knocking and non-knocking populations that are present within the dataset. However, estimates were always performed independently at each crank angle, and no attempt was made to exploit the clear resonant functional form that is evident in the results.

In this work, we therefore take this line of investigation one step further by assuming that the random cyclic variations observed at different crank angles within the same cycle are not independent from one another, but rather result from some perturbation of the deterministic *function* defined by the knock signature. These perturbations, which are assumed to be characterized by small gain and phase shifts, provide a much more concise yet complete description of the data since the stochastic properties of cyclic variation are now captured by the covariance of the perturbation parameters. Such a model then offers possibilities for simulating stochastically similar data sets, or for deriving analytically the results expected from applying different knock detection methods to the data. The

paper is organized as follows: Section 2 briefly reviews the data alignment process, the resulting set of ensemble mean signatures that are obtained for different spark timings relative to BorderLine (BL) knock conditions. A cyclic model, based on perturbation about this set of mean signatures is then proposed and fitted to the data in Section 3. The extent to which this model accurately characterizes the data is assessed and the distribution and covariance of perturbation model parameters is investigated. Finally, brief conclusions are given in Section 4.

2. DATA, AND DATA ALIGNMENT

Data for this study was recorded from a Ford V8 gasoline engine connected to a low inertia dynamometer on an engine testbed. The engine was operated at 1000 rpm, Wide Open Throttle (WOT) using 91 Research Octane Number (RON) fuel, and no Exhaust Gas Recirculation (EGR). A standard powertrain control module was used to regulate all engine variables apart from the spark timing which was stepped at intervals of 1° from BL-3° to BL+2° where BL denotes the angle of BorderLine audible knock. At each spark condition 1002 cycles of data were recorded for analysis. Each cylinder was equipped with a flush-mounted cylinder pressure sensor, so this data included raw pressure signals from all eight cylinders, though the analysis in this work is limited to cylinder #1. An encoder was used to sample data every $1/10^{th}$ of a crank angle degree resulting in a 60 kHz sample rate when operating at 1000 rpm.

To focus on the higher frequency knock components, cylinder pressure measurements are typically bandpass filtered about the knock resonant frequency before further processing. In this work, however, the ensemble mean pressure was first subtracted from each cyclic pressure waveform before applying a broad 4.5 - 15 kHz bandpass filter to the remaining cyclic pressure fluctuation signal. This was found to be more effective at removing the low-frequency deterministic components of the waveform. The data was also forward and reverse filtered through the bandpass filter in order to preserve any phase-related effects.

Typical examples of the resultant filtered pressure fluctuation traces, (Fig. 1), show the resonant ringing associated with knock, as well as significant variations in the response from one cycle to the next. Previous analyses have shown that these variations are cyclically uncorrelated and vary as a stationary random process with respect to cycle number, (J. C. Peyton Jones & Shayestehmanesh, 2021). More generally, these instances belong to a *distribution* of all possible knock signals that are generated at this operating condition. This work aims to capture the statistical properties and characteristics of this distribution and thereby to describe the process more completely and repeatably than is possible using individual / specific instances.

As noted in the introduction, however, the crank-angle dependent properties of these distributions are confounded by random variations in the angle of knock onset. Simply computing the ensemble mean across cycles, as one might when analyzing cylinder pressure, gives a zero mean result as seen in Fig. 2 for the BL+2 dataset (red trace). Even though deterministic resonant characteristics are visible in all of the individual traces of Fig. 1, their random phasing with respect to one another means that they average out rather than combine constructively when computing the ensemble mean.

It is therefore first necessary to align the data relative to some reference cycle, chosen in this case to be from the 98^{th} percentile of the maximum knock oscillation amplitude in the Bl+2 dataset, (J. Peyton Jones & Patel, 2021). The angular delay of knock onset relative to the reference cycle can be estimated from the angle at which the cross-correlation between each individual cycle and the reference cycle, is maximized. The data can then be shifted to 'correct' for cyclic differences in knock onset, and re-evaluating the ensemble mean pressure fluctuation then gives the 'aligned' knock resonant response also shown in Fig. 2 (blue trace). This is a more meaningful and repeatable result than the individual traces of Fig. 1, because it represents the statistically expected knock 'signature' for this dataset. Unlike frequency domain power spectral analyses, it also preserves the time-varying aspects of knock onset, growth and decay, including the slight decrease in resonant frequency with time that is visible as the gas expands and cools. Also note that cyclic noise variations are averaged out, and the response is largely noise-free, despite the fact that no frequency-selective filters have been applied.

Although the ensemble mean response offers a useful way to observe and quantify empirically recorded knock data, it still does not fully characterize the *distribution* of knock pressure signals as they vary from one cycle to the next. More information about the shape of this distribution can be seen by plotting the third order moment or skewness as shown in Fig. 3. Prior to alignment, the dataset is heavily skewed around knock onset since some cycles are already knocking, while others are not, but thereafter the skewness is near zero with no consistent pattern visible in the data. After alignment, however, inspection Fig. 3 clearly shows that the skewness oscillates in synchronicity with the ensemble mean trace, (Fig. 2), being most positively skewed at the maxima of the knock signature, zero-skewed at its zero crossings, and most negatively skewed at its minima.

It should be noted that each point on the waveforms shown in Figs. 2, 3 is estimated independently from its immediate neighbors. The fact that the results yield such smooth results is strong evidence that not only is the mean response functionally determined by knock resonance, but the characteristics of the entire distribution vary deterministically / functionally with crank angle. The objective of this work is to develop a more concise and complete stochastic model for cyclic variations of knock signals which exploits these functional dependencies. (The slight amplitude modulation visible in both aligned and non-aligned data for angles greater than 50° ATDC is likely due to numerical effects when computing the skewness of variations that are by this time very small).

3. FUNCTIONAL MODELING OF CYCLIC VARIATIONS

Prior work modeling the distributions underlying Figs. 2,3, has ignored their evident functional characteristics, and instead modeled the distribution at each crank angle separately. It was shown, for example, that the distribution at any given crank angle can be successfully modeled as a sum of *two* Gaussian distributions representing the knocking and non-knocking populations respectively that are present in the dataset, (J. Peyton Jones & Patel, 2021). The probability density function function $f(\cdot)$ of the observed filtered pressure fluctuations $\Delta P_f(\theta_i)$ at crank angle θ_i can then be expressed as a function of Gaussian model parameters μ_{i1}, μ_{i2}, σ_{i1}, σ_{i2}, pertaining at angle θ_i. This gives,

$$f\left(\Delta P_f(\theta_i)|\mu_{i1},\mu_{i2},\sigma_{i1},\sigma_{i2},p_i\right) = p_i\, f\left(\Delta P_f(\theta_i)|\mu_{i1},\sigma_{i1}\right) + (1-p_i)\, f\left(\Delta P_f(\theta_i)|\mu_{i2},\sigma_{i2}\right) \quad (1)$$

where the quantities p and (1-p) denote the fraction of the total population that belong to the knocking and non-knocking populations respectively, and where $f(x\,|\mu,\sigma)$ denotes a single-Gaussian distribution, used to describe each of these populations in terms of its own mean μ and variance, σ^2.

$$f\left(x|\mu,\sigma\right) = \frac{1}{x\sqrt{2\pi\sigma^2}}\exp\left(\frac{-(x-\mu)^2}{2\sigma^2}\right) \quad (2)$$

This model has proved to be very effective. Not only was it able to accommodate the oscillation between left- and right-skewed distributions that are observed in Fig. 3, but it enabled the ensemble mean response shown in Fig. 2 to be decomposed into its constituent parts representing the knocking and non-knocking signature of the engine at the given operating condition. The estimated variances associated with these populations (not shown for reasons of space) also give insight into the stability of each type of combustion, and the estimated knock fraction, p, provides a useful measure of the proportion of abnormal combustion cycles in the dataset.

Despite these benefits, however, the model represented by (1), (2), is not very parsimonious since it requires 5 parameters for each point of the waveforms shown in Figs. 1-3. With a sampling rate of 1/10th of a crank angle degree, and a region of interest that spans about 50°, it requires around 2500 parameters to fully model the distributions. Even given these parameters, the model is incomplete because it is not possible to use them to generate a sample instance of the observed waveform: One can certainly generate sample instances of the pressure fluctuation at a given crank angle θ_i but there is no reason why the instances obtained at neighboring crank angles should exhibit any smooth / resonant functional form.

An alternative is to assume that the filtered pressure fluctuations at cycle number j and operating condition BL+k° can be described as some functional *expression* $\Delta P_{j,k}(\theta_i,\ \lambda)$, parameterized by a set of variables, λ. In this case we assume that $\Delta P_{j,k}(\theta_i,\ \lambda)$ can be further expanded as some oscillatory function $f_k(\omega_{j,k}\,t_i + \phi_{j,k})$ scaled by an amplitude $A_{j,k}$, giving,

$$\Delta P_{j,k}(\theta_i,\lambda) = A_{j,k} f_k(\omega_{j,k}t_i + \phi_{j,k});\qquad \theta_i = \omega_{j,k}t_i + \phi_{j,k} \quad (3)$$

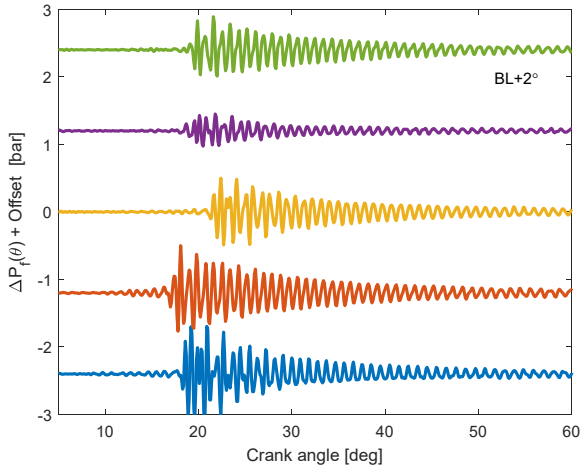

Fig. 1. Typical knock signal waveforms obtained as filtered cylinder pressure fluctuations $\Delta P_f(\theta)$ relative to the ensemble mean pressure.

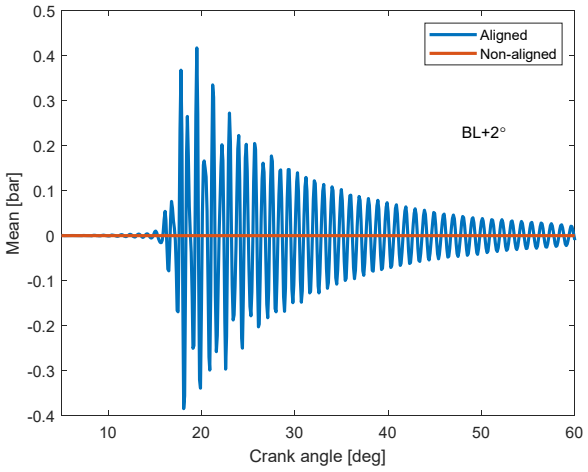

Fig. 2: Ensemble mean of knock signal waveforms, taken across cycles, before and after alignment.

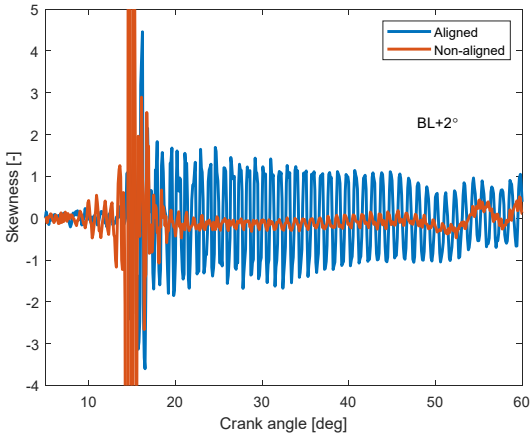

Fig. 3: Skewness of distribution of knock signal waveforms, taken across cycles after alignment.

The pressure fluctuations at each cycle j and operating condition BL+k° therefore all share the same functional form, but may oscillate at a slightly different frequency $\omega_{j,k}$, and (despite the alignment process) be slightly shifted by a phase $\phi_{j,k}$, as well as having a different overall magnitude $A_{j,k}$. Together, these variables define the set of parameters, λ. The

ensemble mean knock signature can also be described in the same way, using an overbar to denote this special case,

$$\overline{\Delta P_k}(\theta_i) = \Delta P_k(\theta_i, \overline{\lambda}) = \overline{A}_k f_k(\overline{\omega}_k t_i + \overline{\phi}_k)$$
$$where\ \overline{A}_k = 1,\ \overline{\phi}_k = 0,\ \overline{\omega}_k = \omega_0 \tag{4}$$

If cyclic variations about the ensemble mean pressure trace are relatively small, then they can be approximated by linearizing (3) with respect to each parameter in the model,

$$\Delta P_{j,k}(\theta_i) = \Delta P_k(\theta_i, \overline{\lambda}) + \sum_{\lambda} \left. \frac{\partial(\Delta P_k(\theta_i, \lambda))}{\partial \lambda_{j,k}} \right|_{\lambda=\overline{\lambda}} \times \Delta\lambda_{j,k} \tag{5}$$

More specifically, this gives in this case,

$$\Delta P_{j,k}(\theta_i, \lambda) = \overline{\Delta P_k}(\theta_i) + \frac{\partial(\overline{\Delta P_k}(\theta_i))}{\partial A_{j,k}} \times \Delta A_{j,k}$$
$$+ \frac{\partial(\overline{\Delta P_k}(\theta_i))}{\partial \theta_i} \frac{\partial \theta_i}{\partial \omega_{j,k}} \times \Delta\omega_{j,k} + \frac{\partial(\overline{\Delta P_k}(\theta_i))}{\partial \theta_i} \frac{\partial \theta_i}{\partial \phi_{j,k}} \times \Delta\phi_{j,k} \tag{6}$$

The required derivatives are obtained from (3) as,

$$\frac{\partial(\Delta P_k(\theta_i))}{\partial A_{j,k}} = f_k(\omega_{j,k} t_i + \phi_{j,k}); \quad \frac{\partial \theta_i}{\partial \omega_{j,k}} = t_i; \quad \frac{\partial \theta_i}{\partial \phi_{j,k}} = 1 \tag{7}$$

Substituting from (4), and using a prime to indicate differentiation with respect to θ, the final linearized expression is given by,

$$\Delta P_{j,k}(\theta_i) = \overline{\Delta P_k}(\theta_i)\left(1 + \Delta A_{j,k}\right)$$
$$+ t_i \overline{\Delta P}'_k(\theta_i) \times \Delta\omega_{j,k} + \overline{\Delta P}'_k(\theta_i) \times \Delta\phi_{j,k} \tag{8}$$

This expression is useful because it decomposes cyclic variations into small parametric variations in amplitude, frequency and phase that are applied to the known ensemble mean response and its derivative with respect to crank angle. Given multiple observations over an angular region of interest, $[\theta_1, \ldots, \theta_n]$, (8) can be written in matrix form as,

$$\Delta\hat{\mathbf{P}}_{j,k} = \mathbf{\Phi}\ \Delta\boldsymbol{\lambda} \tag{9}$$

where the ith element of the pressure fluctuation time history vector $\mathbf{\Delta P}_{j,k}$ is $\Delta P_{j,k}(\theta_i)$ and where the regressors, $\mathbf{\Phi}$, and parameter vector, $\boldsymbol{\lambda}$, are defined as,

$$\mathbf{\Phi} = \begin{pmatrix} \overline{\Delta P_k}(\theta_1) & t_1 \overline{\Delta P'_k}(\theta_1) & \overline{\Delta P'_k}(\theta_1) \\ \vdots & \vdots & \vdots \\ \overline{\Delta P_k}(\theta_n) & t_n \overline{\Delta P'_k}(\theta_n) & \overline{\Delta P'_k}(\theta_n) \end{pmatrix},$$
$$\Delta\boldsymbol{\lambda} = \begin{pmatrix} 1 + \Delta A_{j,k} & \Delta\omega_{j,k} & \Delta\phi_{j,k} \end{pmatrix}^T \tag{10}$$

The unknown cyclic parameter variations, $\Delta A_{j,k}$, $\Delta\omega_{j,k}$, $\Delta\phi_{j,k}$, (which represent the variations in amplitude, frequency and phase of the oscillation (3), relative to their ensemble mean values), are then readily estimated using least squares with the ensemble knock signature and its derivative as regressors and repeating the process for each cycle, j, in the specified dataset BL+k°. A plot of the resulting fit for the five example cycles considered in Fig. 1, is shown in Fig. 4, and the corresponding residuals are shown in Fig. 5. Despite the substantial cyclic variability evident in Fig. 1, the model is reasonably effective at characterizing each trace, and the magnitude of the residuals

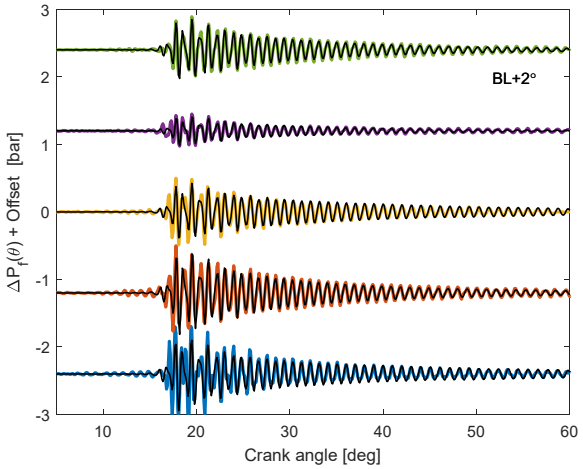

Fig. 4. Original and fitted knock signal waveforms.

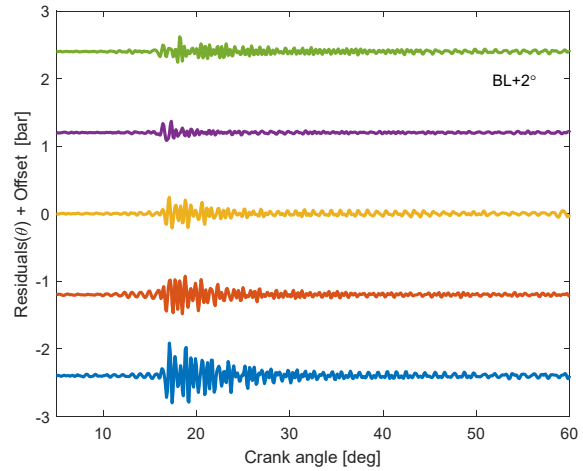

Fig. 5: Unmodelled residuals after model fitting.

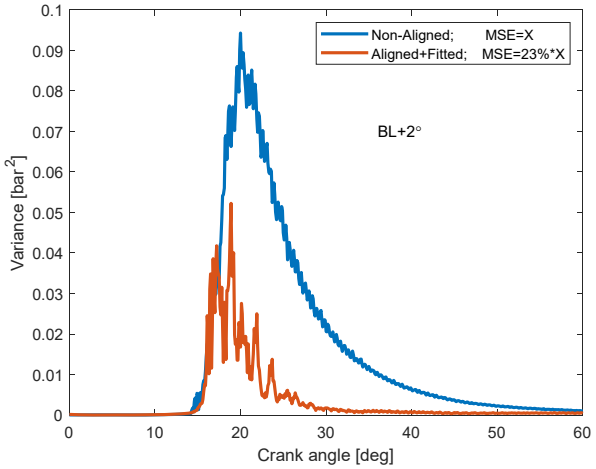

Fig. 6: Variance of the residuals and of the original knock signal waveforms, taken across cycles.

is relatively small. Some discrepancies can be seen in the high intensity region immediately following knock onset, but the resonant decay is captured very closely.

A more quantitative assessment of the model fit and its dependence on crank angle can be obtained by plotting the variance of the residuals taken across cycles, as shown in Fig. 6. Also shown in the figure, for comparison is the variance of the original knock signals before the model was fitted. The area under these figures corresponds to the overall mean squared error of the unmodelled component. Overall, the model is seen to significantly reduce the mean squared error to 23% of its original value. As noted above, the fit is best in the resonant decay region after about 25° ATDC, with larger errors in the region immediately following knock onset. Interestingly, the magnitude of the residuals in this region seems to oscillate at some lower frequency despite the fact that low frequency content was removed during the initial filtering of the cylinder pressure signal. It is surmised that maybe two closely spaced knock frequencies may be intermodulating to produce a small beat frequency effect. Indeed, some evidence of this is visible in the time history traces of Fig. 1.

Generally, however, the results suggest that the ensemble mean knock waveform, together with linearized model, (8), successfully capture both the deterministic and stochastic aspects of the knock process. Indeed, the stochastic variations are now encapsulated in the cyclically varying values of the estimated parameters and the distribution of these variables (shown in Figs. 7,8,9) therefore reflects the cyclic distribution of knock waveforms.

The distribution of $\Delta\phi$, shown in Fig. 9, appears reasonably Gaussian. The standard deviation is 0.043 rad or 2.46°, suggesting that most cycles have a relatively small phase offset of less than 5°. The distribution of $\Delta\omega$ is also reasonably symmetric, but with notably thicker tails than one would expect for a Gaussian distribution. The standard deviation is 6.0 Hz, and most cycles fall within 12 Hz of the mean. Since the dominant resonant frequency in the ensemble mean trace (Fig. 2 blue trace) is 6.7 kHz, this represents a ±0.18% variation relative to this reference.

In contrast to Figs. 8, 9, the distribution of ΔA, shown in Fig. 7 is distinctly non-Gaussian, and seems more similar to a log-normal distribution. Indeed, since the value $(1+\Delta A)$ scales the magnitude of the knock waveform, it is perhaps not surprising that it shows a similar distribution to scalar knock metrics such as MAPO which are often assumed to be log-normally distributed, (Naber et al., 2006; J. M. Spelina, Peyton Jones, & Frey, 2013). Unlike a true log-normal distribution, however, the left-most tail of the distribution in Fig. 7 shows that a small number of cycles are scaled by a small, but *negative*, value. This is likely caused by very low-amplitude / non-knocking waveforms in the dataset which are hard to align or fit with any certainty.

Of course, the marginal distributions shown in Figs. 7,8,9 are not necessarily independent of one another. This interdependence is captured by the parameter covariance

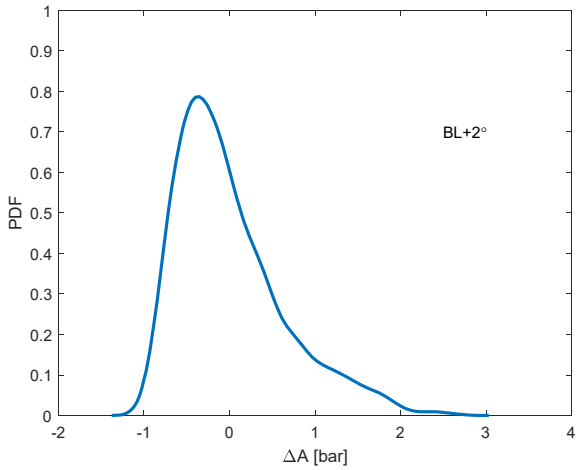

Fig. 7. Distribution of the estimated parameter, $\Delta A_{j,2}$

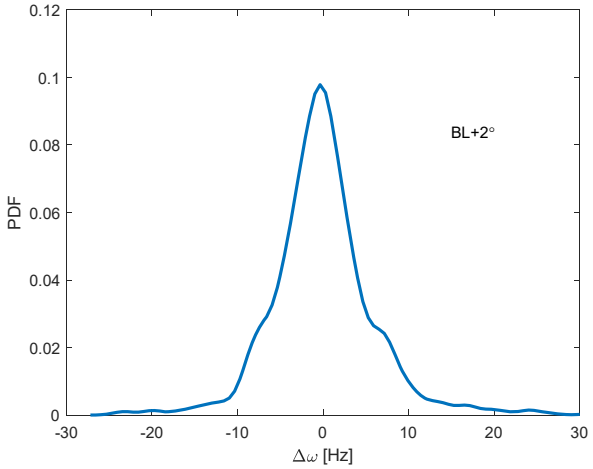

Fig. 8. Distribution of the estimated parameter, $\Delta\omega_{j,2}$

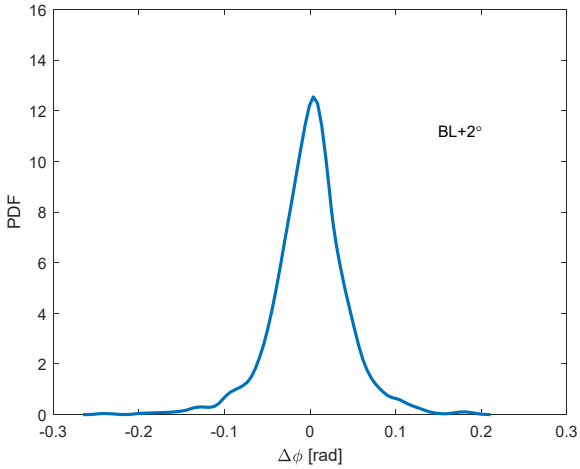

Fig. 9. Distribution of the estimated parameter, $\Delta\phi_{j,2}$

matrix $\mathrm{cov}(\Delta\lambda_j)$ that is automatically computed during least squares estimation. The result of averaging this covariance matrix across all cycles for the BL+2° dataset gives,

$$\frac{1}{N}\sum_{j=1}^{N}\mathrm{cov}(\Delta\lambda_j)=\begin{pmatrix}0.39 & 0.50 & -0.00\\ 0.50 & 34.10 & -0.14\\ -0.00 & -0.14 & 0.00\end{pmatrix} \tag{11}$$

The elements on the leading diagonal represent the variance of each estimated parameter, as already discussed above. Normalizing by these variances gives the corresponding correlation matrix,

$$\frac{1}{N}\sum_{j=1}^{N}\mathrm{corr}(\Delta\lambda_j) = \begin{pmatrix} 1 & 0.14 & -0.03 \\ 0.14 & 1 & -0.54 \\ -0.03 & -0.54 & 1 \end{pmatrix} \quad (12)$$

and the off-diagonal elements then show the correlation of one parameter with another. Inspection of (12) for example shows that positive variations in amplitude are weakly correlated with positive variations in frequency, suggesting that higher intensity cycles are slightly associated with higher temperatures and frequency as one might expect from the physics of the process. Both amplitude and frequency are also negatively correlated with phase, suggesting that such higher intensity cycles also tend to occur slightly earlier in the cycle.

4. CONCLUSIONS

Knock signals display both deterministic (resonant) and stochastic (cyclic) characteristics which together reflect the underlying knock process. This work has shown that both these aspects can be modeled in terms of small variations in amplitude, frequency and phasing of the aligned ensemble mean knock resonant waveform. By fitting the model to the data the stochastic variations of entire knock waveforms are encapsulated very concisely in the variation of the estimated parameters – or more specifically in their distribution and covariance. More work is required to explore how stochastic knock behavior, as now characterized by this model, varies with spark advance and engine operating condition. In future work, it is also hoped to use the model to simulate knocking waveforms whose statistical properties match those of the original data from which the model was derived. Finally, it is hoped that the improved / stochastic understanding of knock signal waveforms may provide a more informed basis for developing improved knock detection algorithms.

REFERENCES

Brecq, G., & Le Corre, O. (2005). Modeling of In-cylinder Pressure Oscillations under Knocking Conditions: Introduction to Pressure Envelope Curve. *SAE Technical Paper*, (2005-01–1126). https://doi.org/10.4271/2005-01-1126

Di Gaeta, A., Giglio, V., Police, G., & Rispoli, N. (2013). Modeling of in-cylinder pressure oscillations under knocking conditions: A general approach based on the damped wave equation. *Fuel*, *104*, 230–243. https://doi.org/10.1016/j.fuel.2012.07.066

Draper, C. S. (1938). Pressure waves accompanying detonation in the internal combustion engine. *J Aeronautical Sciences*, *5*(6), 219–226.

Heywood, J. B. (1988). *Internal combustion engine fundamentals*. New York City: McGraw-Hill Education.

Lee, J., Hwang, S., Lim, J., Jeon, D.-C., & Cho, Y.-S. (1998). A New Knock-Detection Method using Cylinder Pressure, Block Vibration and Sound Pressure Signals from a SI Engine. *SAE Transactions - Journal of Engines*, *107–3*(981436). https://doi.org/10.4271/981436

Millo, F., & Ferraro, C. (1998). Knock in S.I. engines: a comparison between different techniques for detection and control. *SAE Transactions - Journal of Fuels and Lubricants*, *107(4)*(982477). https://doi.org/10.4271/982477

Naber, J. D., Blough, J. R., Frankowski, D., Goble, M., & Szpytman, J. E. (2006). Analysis of Combustion Knock Metrics in Spark-Ignition Engines. *SAE Transactions Journal of Engines*, *115(3)*(2006-01–0400). https://doi.org/10.4271/2006-01-0400

Pan, J., Shu, G., & Wei, H. (2014). Research on in-cylinder pressure oscillation characteristic during knocking combustion in spark-ignition engine. *Fuel*, *120*, 150–157. https://doi.org/10.1016/j.fuel.2013.11.054

Peyton Jones, J. C., & Shayestehmanesh, S. (2021). The statistical properties of raw knock signal time histories. *Mechanical Systems and Signal Processing*, *156*, 107660. https://doi.org/10.1016/j.ymssp.2021.107660

Peyton Jones, J., & Patel, V. (2021). The statistical characteristics of knock signal waveforms. *International Journal of Engine Research*. https://doi.org/10.1177/14680874211034403

Scholl, D., Davis, C., Russ, S., & Barash, T. (1998). The Volume Acoustic Modes of Spark-Ignited Internal Combustion Chambers. *SAE Transactions - Journal of Engines*, *107(3)*(980893). https://doi.org/10.4271/980893

Shahlari, A. J., & Ghandhi, J. B. (2012). A Comparison of Engine Knock Metrics. *SAE Technical Paper*, (2012-32–0007). https://doi.org/10.4271/2012-32-0007

Spelina, J. M., Peyton Jones, J. C., & Frey, J. (2013). Characterization of knock intensity distributions: Part 2: parametric models. *Proceedings of the Institution of Mechanical Engineers, Part D: Journal of Automobile Engineering*, *227*(12), 1650–1660. https://doi.org/10.1177/0954407013496234

Spelina, Jill. M., Peyton Jones, J. C., & Frey, J. (2014). Characterization of knock intensity distributions: Part 1: statistical independence and scalar measures. *Journal of Automobile Engineering*, *228*(2), 117–128. https://doi.org/10.1177/0954407013496233